Cancer Research

RORγt$^+$ Innate Lymphoid Cells Promote Lymph Node Metastasis of Breast Cancers

Sheeba Irshad[1], Fabian Flores-Borja[1,2], Katherine Lawler[2,3], James Monypenny[2], Rachel Evans[2], Victoria Male[1], Peter Gordon[1,2], Anthony Cheung[2], Patrycja Gazinska[1], Farzana Noor[1], Felix Wong[2], Anita Grigoriadis[1], Gilbert O. Fruhwirth[2,4], Paul R. Barber[5], Natalie Woodman[6], Dominic Patel[7], Manuel Rodriguez-Justo[7], Julie Owen[6], Stewart G. Martin[8], Sarah E. Pinder[6,9], Cheryl E. Gillett[6,9], Simon P. Poland[2], Simon Ameer-Beg[2], Frank McCaughan[10,11], Leo M. Carlin[4], Uzma Hasan[7], David R. Withers[12], Peter Lane[12], Borivoj Vojnovic[5], Sergio A. Quezada[13], Paul Ellis[14], Andrew N.J. Tutt[1,15], and Tony Ng[1,2,13]

Abstract

Cancer cells tend to metastasize first to tumor-draining lymph nodes, but the mechanisms mediating cancer cell invasion into the lymphatic vasculature remain little understood. Here, we show that in the human breast tumor microenvironment (TME), the presence of increased numbers of RORγt$^+$ group 3 innate lymphoid cells (ILC3) correlates with an increased likelihood of lymph node metastasis. In a preclinical mouse model of breast cancer, CCL21-mediated recruitment of ILC3 to tumors stimulated the production of the CXCL13 by TME stromal cells, which in turn promoted ILC3–stromal interactions and production of the cancer cell motile factor RANKL. Depleting ILC3 or neutralizing CCL21, CXCL13, or RANKL was sufficient to decrease lymph node metastasis. Our findings establish a role for RORγt$^+$ILC3 in promoting lymphatic metastasis by modulating the local chemokine milieu of cancer cells in the TME. *Cancer Res; 77(5); 1083–96. ©2017 AACR.*

Introduction

Breast cancer is the most common malignant neoplasm with significant morbidity and mortality. The ability of cancer cells to invade lymphatics stratifies breast cancers into distinct prognostic groups (1). The molecular mechanisms mediating this tumor cell entry remain unclear, but studies have established important roles for the lymphoid chemokines CXCL13, CCL19, and CCL21 (2).

An important early step in the construction of lymphoid organs is the recruitment of lymphoid tissue inducer cells (LTi) by CXCL13 and CCL21, which are recognized via the receptors CXCR5 and CCR7, respectively (3–5). LTis are members of the innate lymphoid cells (ILC) family. Recent moves to propose a uniform nomenclature divide these cells into three groups (6), and LTis represent the prototypic cell type of the "group 3" RORγt$^+$ family of ILCs. We will refer to these cells henceforth as ILC3. ILC3 play a major role in lymphoid tissue development both in the embryo (7) and in adult life (8, 9). Within the secondary lymphoid structures, ILC3 produce lymphotoxin (LT)$\alpha_1\beta_2$, which binds LTβR on mesenchymal stromal cells (MSC), stimulating the production of CXCL13, CCL19, and CCL21, as well as the TNF family member, RANKL, promoting lymphocyte recruitment and compartmentalization (10).

The presence or role of these cells has not yet been explored in breast cancers. Here, we demonstrate that CCL21-dependent recruitment of ILC3s into mammary tumors results in a

[1]Breast Cancer Now (BCN) Research Unit, King's College London, London, United Kingdom. [2]Richard Dimbleby, Randall Division & Division of Cancer Studies, King's College London, London, United Kingdom. [3]Institute for Mathematical and Molecular Biomedicine, King's College London, London, United Kingdom. [4]Leukocyte Dynamics Group, Beatson Advanced Imaging Resource, CRUK Beatson Institute, Glasgow, United Kingdom. [5]Gray Institute for Radiation Oncology & Biology, University of Oxford, Oxford, United Kingdom. [6]King's Health Partners Cancer Biobank, King's College London, London, United Kingdom. [7]International Center for Infectiology Research, University of Lyon, Lyon, France. [8]Division of Cancer and Stem Cells, Department of Clinical Oncology, School of Medicine, Nottingham University Hospitals NHS Trust, Nottingham, United Kingdom. [9]Research Oncology, Division of Cancer Studies, King's College London, Guy's Hospital, London, United Kingdom. [10]Department of Asthma, Allergy, and Lung Biology, King's College London, London, United Kingdom. [11]Department of Biochemistry, University of Cambridge, Cambridge, United Kingdom. [12]MRC Centre for Immune Regulation, Institute for Biomedical Research, College of Medical and Dental Sciences, University of Birmingham, Birmingham, United Kingdom. [13]UCL Cancer Institute, Paul O'Gorman Building, University College London, London, United Kingdom. [14]Department of Medical Oncology, Guy's and St Thomas Foundation Trust, London, United Kingdom. [15]ICR, BCN Research Unit, Toby Robins Research Centre, London, United Kingdom.

Note: Supplementary data for this article are available at Cancer Research Online (http://cancerres.aacrjournals.org/).

S. Irshad and F. Flores-Borja contributed equally to this article.

Corresponding Author: Tony Ng, King's College London, 2nd Floor, Rm 2.32d (Office), London SE1 1UL, United Kingdom. Phone: 4402-0784-88056; Fax: 4402-0784-86435; E-mail: tony.ng@kcl.ac.uk

doi: 10.1158/0008-5472.CAN-16-0598

CXCL13-dependent positive feedback loop between ILC3 and MSCs. Antibody-blocking experiments in BALB/c and Rag1$^{-/-}$ mice demonstrated that CCL21, CXCL13, ILC3, and RANKL all promote metastasis to the lymph node. We report the novel identification of RORγt^{+}ILC3s within the human tumor microenvironment, their association with more agressive breast cancer subtypes, and lymphatic metastasis.

Materials and Methods

Human tissue

Tissue samples and data from patients were obtained from The King's Health Partners (KHP) Cancer Biobank at Guy's Hospital (London, United Kingdom; REC nr.: 07/40874/131).

Mice

Experiments were performed in accordance with the UK Home Office Animals Scientific Procedures Act, 1986 and the UKCCCR guidelines. Tumors were established by the injection of 4T1.2 cells into the mammary fat pad of 6- to 8-week-old BALB/c mice (Charles River Laboratories) and Rag1$^{-/-}$ mice (BALB/c background, The Jackson Laboratory). CXCL13 or CCL21 were neutralized by intravenous injection of 0.5 μg goat antibodies (R&D Systems) starting on the first day after tumor establishment and repeated every 3 days until the end of the experiment. ILCs were depleted by intraperitoneal injection of 0.25 mg anti-CD90.2 (clone 30H12, Bio X Cell) starting on day 3 after tumor establishment and repeated every 3 days until the end of the experiment.

Gene expression datasets

The KHP Cancer Biobank of the Molecular Taxonomy of Breast Cancer International Consortium (METABRIC) dataset was profiled using the Illumina HT12 platform. Frozen tissue sections were subjected to histopathologic review to assess the presence of invasive tumor, and only samples with >70% tumoral DNA were included. Samples were quantile normalized, and a ComBat BeadChip correction applied [$N = 234$; 176 estrogen receptor–positive (ER^{+}) samples, 58 ER^{-} samples]. PAM50 subtype was assigned as in refs. 11–13.

IHC, immunofluorescence, and image analysis

Sixty fresh-frozen tumor sections were randomly selected from the METABRIC patient cohort for ILC staining as described previously (14). Confocal tile scan images were obtained using an LSM510 Metamicroscope (Carl Zeiss). Image analysis for RORγt^{+}ILC quantification was carried out using MacBiophotonics ImageJ software. Detailed IHC protocols are described in Supplementary Information.

Cell lines and culture conditions

The mouse breast cancer cell line 4T1.2 (derived from a mammary carcinoma in a BALB/c mouse; ref. 15) and human bone marrow–derived MSCs (HS-5) were cultured in DMEM (Invitrogen) complete media. Extracellular matrix (ECM) invasion assays, based on the Boyden chamber principle, were carried out using 96-well Cell Invasion Assay Kit (ECM555, Chemicon International) as per the manufacturers' instructions. To confirm identity, short tandem repeat profiling was performed on all cell lines.

ILC3 cell isolation and flow cytometry

For NKp46^{-}ILC3 sorting experiments, splenocyte suspensions were prepared from BALB/c mice and cells stained with CD3, CD11c, B220R, CD127, CD90.2, and NKp46 and sorted by using a FACSAria. The NKp46^{-}ILC3 were identified as CD3^{-}CD11c^{-}B220^{-}CD127^{+}CD90.2^{+}NKp46^{-} cells. Purity was confirmed at >90%. To extract intratumoral ILC3, tumors were minced and incubated with collagenase/hyaluronidase at 37°C for 60 minutes and passed through a filter to form a single-cell suspension. Cells were stained as per sorting experiments. Flow cytometry reference beads (PeakFlow blue; Invitrogen) were added to the samples before analysis for quantification of cells in each tumor. The absolute number of cells/mg of tumor was calculated using the formula: density of x cells = (number of beads added to each sample multiplied by count of x cells/count of beads)/tumor weight. For multi-photon experiments, 5–6 $\times$ 10^4 sorted NKp46^{-}ILC3 were injected (intravenously) into tumor-bearing mice on the same day. Immune cell populations from tumors and draining lymph nodes (DLN) from mice after treatment with either neutralizing anti-CXCL13, anti-CCL21, or IgG control (R&D Systems) were isolated as described above. Antibodies used are included in Supplementary Table S1.

Time-lapse microscopy and image analysis

Cells were cultured in DMEM complete medium supplemented with 25 mmol/L HEPES. For NKp46^{-}ILC3-MSC coculture experiments, MSCs were grown in 9.4 $\times$ 10.7 mm ibidi 8-well slide chambers. Image acquisition was performed using an Olympus IX71 inverted microscope housed within an environment chamber maintained at 37°C. Sequential phase contrast images were captured every 10 minutes for a total of 10 hours. NKp46^{-}ILC3-MSC clustering was measured as described in Supplementary Information.

ELISA

Tumors were snap frozen and lysed by homogenization in 100 mmol/L Tris pH 7.5, 150 mmol/L NaCl, 1 mmol/L EGTA, 1 mmol/L EDTA, 1% (v/v) Triton X-100, and 0.5% (w/v) sodium deoxycholate. ELISAs were performed using DuoSet Kits (R&D Systems).

siRNA knockdown

MSCs were cultured overnight in 6-well plates to 30% confluency. Cells were transfected with RNAiMAX in serum-free OptiMEM and siRNAs at 20 nmol/L. Details of the siRNA used are in Supplementary Table S2.

Surgical window and multi-photon imaging

Mammary imaging window (MIW) surgery was performed 10 days after injection of 1 $\times$ 10^6 4T1.2 cells into the mammary fat pad as described previously (16). For multi-photon experiments, 1 $\times$ 10^6 MSCs (control or knockdown) followed 24 hours later by 5 $\times$ 10^4 sorted NKp46^{-}ILC3 cells were intravenously injected into mice. Twenty-four hours later, mice were placed in a microscope-attached imaging box kept at 32°C and imaged for a maximum period of 3 hours/day for 3 consecutive days. Image processing and image reconstructions were done using MacBiophotonics ImageJ software.

Statistical analysis

Permutation tests for small samples with multiple ties were performed using the "coin" package in R-2.13.0 (17). Predictive value of ILC score for high lymph node burden was determined using Cox multivariate proportional hazards model. GraphPad was used for other data analysis. P values <0.05 were considered significant.

Results

CCL21-mediated recruitment of NKp46$^-$ILC3 to tumors in a mouse model of triple-negative breast cancer

To investigate whether ILC3s are recruited into a TME, we used a mouse model of triple-negative breast cancer (TNBC) with 4T1.2 cells in BALB/c mice that develop metastatic disease via lymphatics (Fig. 1A; ref. 18). Upon tumor induction, the number of NKp46$^-$ILC3 (19) were determined at different times in tumors, DLNs, and nondraining lymph nodes (NDLN; Fig. 1A and B). FACS and immunofluorescence staining for CCR6, RORγt, and CD4 further confirmed the gated cells to be ILC3 (Supplementary Fig. S1). The number of NKp46$^-$ILC3 cells in tumors peaked at day 14 (day 10 vs. day 14, $P = 0.0019$, unpaired t test), whereas the number in DLN peaked later, at day 18 (day 10 vs. day 18, $P = 0.0041$ unpaired t test; Fig. 1B). NKp46$^-$ILC3 cell density within the NDLN did not change significantly, acting as an internal control. Confocal imaging of primary tumors and DLNs taken at day 14 and day 21, respectively, for markers discriminatory for RORγt$^+$ILC3 (defined as RORγt$^+$CD127$^+$CD3$^-$) as previously published (20) confirmed the presence within our mouse model (Fig. 1C and D). In contrast to the temporal pattern of NKp46$^-$ILC3 infiltration (Fig. 1B), absolute numbers of CD3$^+$ T cells (Fig. 1E) and CD19$^+$ B cells (Fig. 1F) decreased in tumors over time, whereas the number of T and B cells in the DLN continued to increase until day 24.

CXCL13 has an essential role in ILC3 function (5), and lymphoid structures resembling the LN paracortex develop in tumors expressing high levels of CCL21 (21). Therefore, we investigated whether either of these chemokines could play a role in the recruitment of NKp46$^-$ILC3 cells to tumors in our model. We confirmed that tumor NKp46$^-$ILC3 express both CCR7 and CXCR5 and are thus capable of responding to CCL21 and CXCL13, respectively (Fig. 1G). We then analyzed the levels of CCL21 and CXCL13 present in primary tumors and serum at various times after tumor establishment. CCL21 levels peaked in both the tumor and serum at day 12, before declining rapidly (Fig. 1H). CXCL13 in the tumor also peaked early (day 10–12), but levels in serum lagged behind, peaking at day 14. In contrast to CCL21, CXCL13 oscillated, with tumor CXCL13 beginning to rise again at day 20 and serum CXCL13 concentration increasing at day 24 (Fig. 1I).

To examine the effect of CCL21 or CXCL13 blockade on NKp46$^-$ILC3 recruitment to tumors *in vivo*, tumor-bearing mice were treated with control or neutralizing anti-CXCL13 and anti-CCL21 antibodies, starting one day after tumor cell implantation and repeated every 3 days. Tumors were analyzed for NKp46$^-$ILC3 at day 14, a time point at which maximum number of these cells had previously been shown to be present in the tumors (Fig. 1B). When compared with isotype controls, anti-CCL21, but not anti-CXCL13 neutralizing antibodies, significantly reduced NKp46$^-$ILC3 recruitment to the primary tumor (Fig. 1J).

CXCL13 is required for clustering of NKp46$^-$ILC3 and MSC

During embryogenesis, clustering of NKp46$^-$ILC3s and production of CXCL13 and CCL21 by activated lymphoid tissue organizer cells (LTo, closely linked to stromal cells of mesenchymal origin; ref. 22) are responsible for initiating a feedback loop with further NKp46$^-$ILC3 recruitment and subsequent amplification of LT receptor signaling (23). Given the lineage relationship between MSCs, which exhibit a marked tropism for tumors (24), and LTo cells that are known to interact with ILC3s, we hypothesized that ILC3 interaction with CXCL13-producing stromal cells may modulate the chemokine profile of the TME. Within our *in vitro* model, MSCs secrete high concentrations of CCL21 and CXCL13 chemokines (Supplementary Fig. S2).

Time-lapse microscopy demonstrated NKp46$^-$ILC3-MSC clustering (Fig. 2A, top; Supplementary Video S1), with cells remaining closely associated for as long as 7 hours (Fig. 2A, red arrow in bottom; Supplementary Video S2). There was no effect on proliferation of ILC3 on contact or coculture with MSCs (Supplementary Fig. S3A). We quantified cell clustering of NKp46$^-$ILC3-MSC (Fig. 2B) and investigated how knockdown of CXCL13 and CCL21 in MSC (Supplementary Fig. S3B and S3C) affected this clustering rate. Transient siRNA knockdown of CXCL13, but not of CCL21, resulted in a decrease of NKp46$^-$ILC3-MSC clustering around ($P < 0.0001$, unpaired t test; Fig. 2C). CXCL13-mediated clustering may be synergistic with the initial CCL21-mediated recruitment of NKp46$^-$ILC3 into the primary tumor, as the CCL21-recruited NKp46$^-$ILC3 are required to promote significant CXCL13 production by interaction with MSC.

Next, we used an intravital MIW with multi-photon imaging to assess NKp46$^-$ILC3-MSC interaction *in vivo* (16). These visualization experiments were conducted to demonstrate how the fluorescent MSCs (which are allogenic and therefore could have a finite half-life once injected *in vivo*) may interact with ILC in the relatively short term and whether this interaction is CXCL13 dependent. 4T1.2 cells were injected into the mammary fat pad and an MIW placed over the tumor 10 days after inoculation (Fig. 2D, i). Tumor-bearing mice were treated with either neutralizing anti-CXCL13 or isotype antibody (as described for Fig. 1H). Fluorescently labeled MSCs and NKp46$^-$ILC3 were intravenously injected 48 or 24 hours prior to imaging, respectively (Fig. 2D, ii). In control antibody-treated mice, NKp46$^-$ILC3 were clustered and in close proximity to MSCs. However, in mice injected with neutralizing anti-CXCL13 antibody, NKp46$^-$ILC3 and MSCs were not close with each other ($P < 0.0001$, unpaired t test, Fig. 2E and F). These *in vivo* imaging results support the *in vitro* observation that NKp46$^-$ILC3-MSC clustering is CXCL13 dependent.

CCL21, CXCL13, and NKp46$^-$ILC3 cells promote metastasis of tumor cells to DLN

To test the hypothesis that CCL21 and CXCL13 might play a role in promoting metastasis of tumor cells to lymph node, we treated 4T1.2 tumor-bearing mice with neutralizing antibodies against CCL21 or CXCL13, or with an antibody to deplete NKp46$^-$ILC3 and examined the DLN for evidence of metastasis.

In vivo, neither anti-CXCL13 nor anti-CCL21 treatments affected tumor growth (Fig. 3A). The weight of the DLNs were significantly reduced in both cohorts (anti-CXCL13 $P = 0.0156$; and

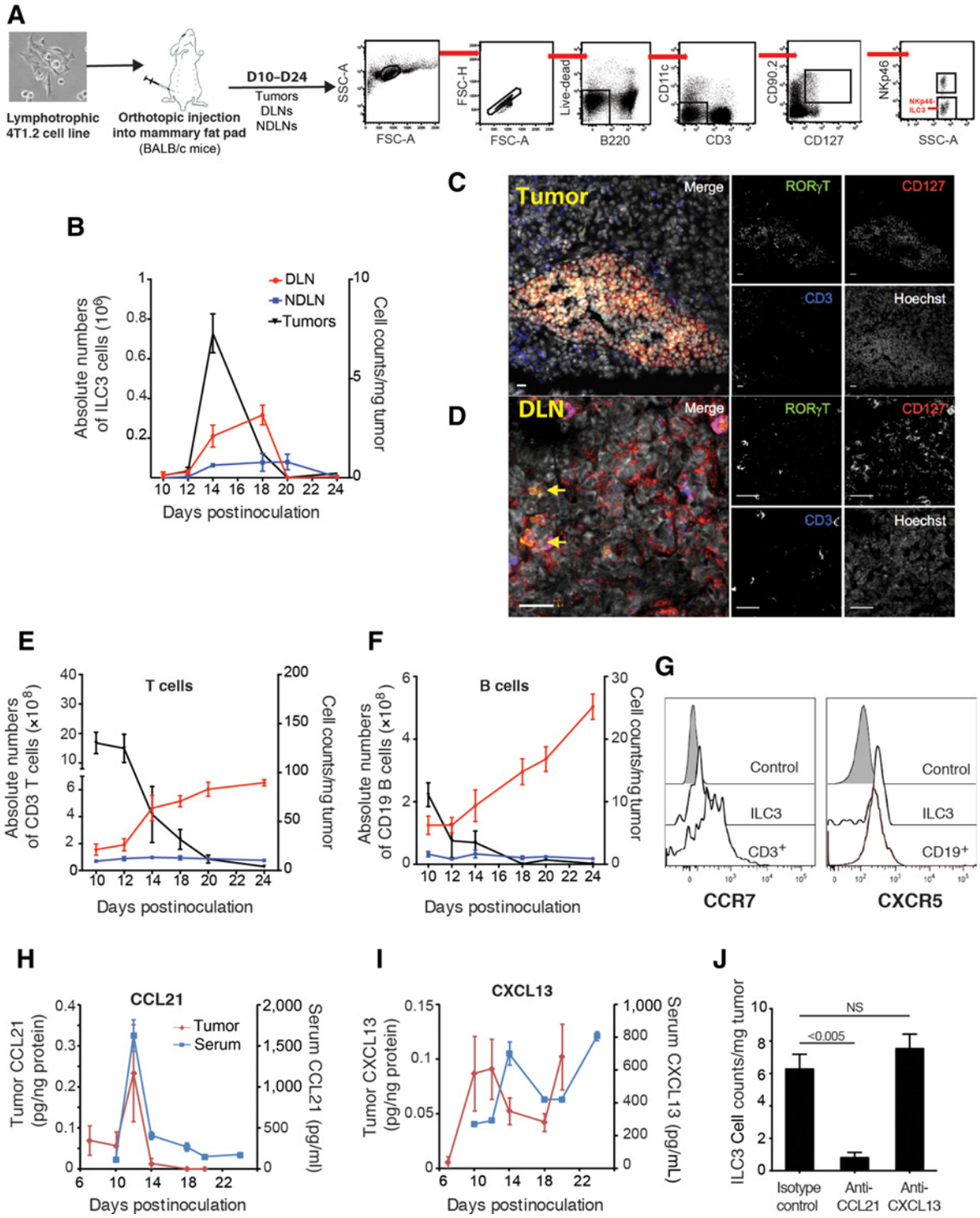

Figure 1.

CCL21 recruits NKp46$^-$ILC3 to tumors in a model of TNBC. **A,** Mice were inoculated subcutaneously with 10^6 4T1.2 cells on day 0. Control and tumor-bearing mice were culled on days 10, 12, 14, 18, 20, and 24. FACS analysis for NKp46$^-$ILC3, CD3$^+$ T, and CD19$^+$ B cells in tumors, DLNs, and NDLNs (n = 3/day). **B,** Absolute number of NKp46$^-$ILC3 in DLN and NDLN and cell counts/mg of tumor. **C** and **D,** Confocal micrographs of primary (**C**) tumor and DLN (**D**) in BALB/c mice. Yellow arrows, ILC3. Scale bars, 15 μm. **E** and **F,** Absolute number of CD3$^+$ T cells (**E**) and CD19$^+$ B cells (**F**) in DLN and NDLN and cell counts/mg of tumor. **G,** CCR7 and CXCR5 expression by intratumoral ILC3, CD3$^+$, and CD19$^+$ cells. **H** and **I,** Levels of CCL21 (**H**) and CXCL13 (**I**) in tumors and serum at indicated time points ($n \geq 3$/time point). **J,** NKp46$^-$ILC3/mg of tumor at day 14 after tumor cell implantation, treated with anti-CCL21, anti-CXCL13, or isotype control antibody ($n \geq 3$). NS, not significant. Significance determined by one-way ANOVA and data represent means ± SEM.

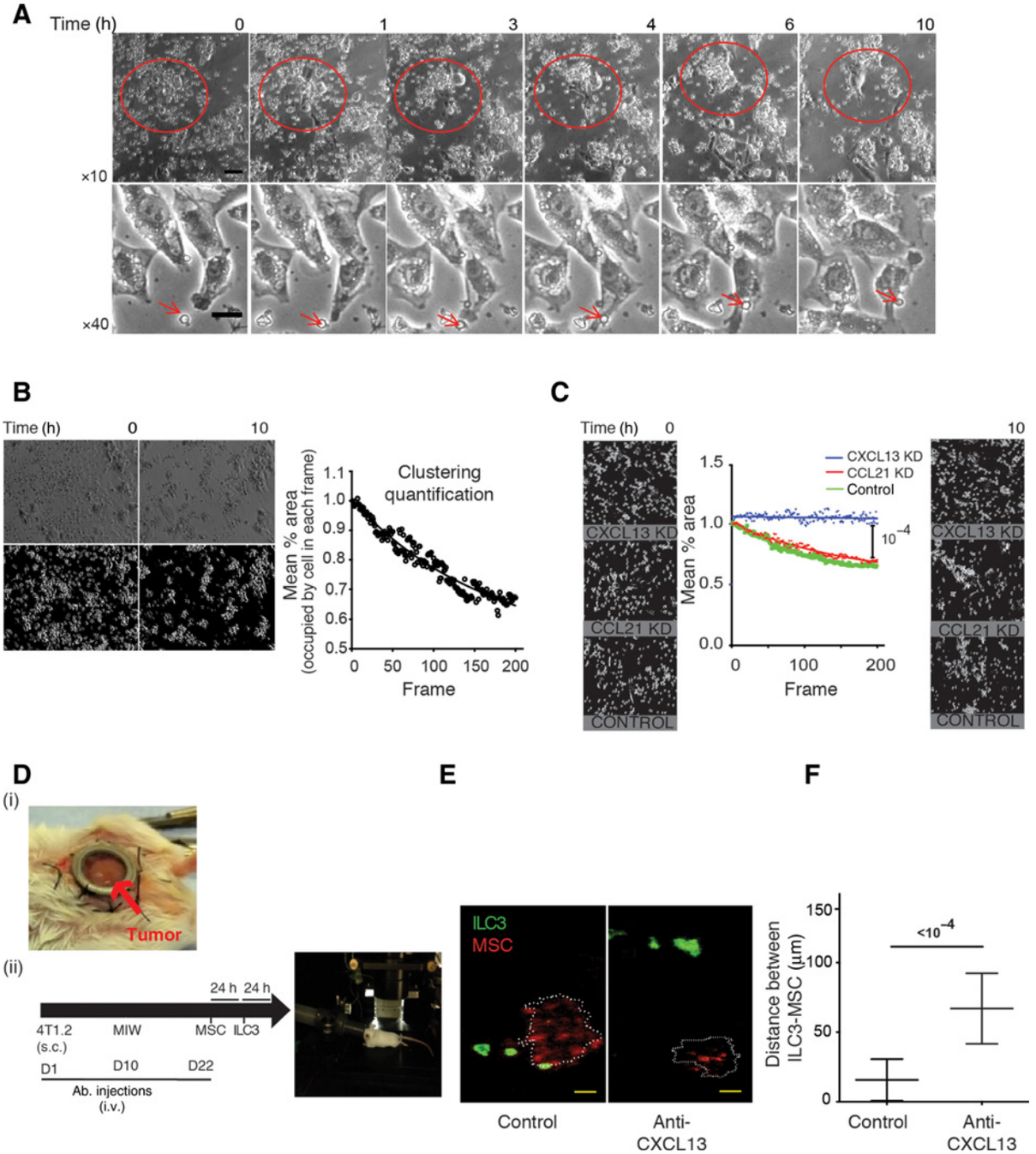

Figure 2.

CXCL13 is required for clustering of NKp46$^-$ILC3 and MSC *in vitro* and *in vivo*. **A,** Time-lapse microscopy of sorted splenic ILC3 cocultured with MSC. Scale bars, 50 (top) and 20 μm (bottom). **B,** Representative phase-contrast (top) and binary images (bottom) used for the quantification of cell clustering. The graph summarizes the change in mean area of the field occupied by cells. **C,** NKp46$^-$ILC3 cocultured with MSC transfected with siRNA targeting CCL21, CXCL13, or control vector. **D, (i),** MIW was surgically implanted on top of the developing tumor; **(ii)** schematic representation of the experimental plan for multi-photon imaging of MSC-NKp46$^-$ILC3 cell interaction. **E,** Representative images ($n = 15$ fields analyzed). Scale bar, 10 μm. **F,** Mean distances between the center of imaged MSCs and NKp46$^-$ILC3 are shown. Significance was determined using unpaired *t* tests.

anti-CCL21 $P = 0.0017$ one-way ANOVA) compared with the control cohort (Fig. 3B). Immunohistochemical analysis of DLN for tumor load with anti-pan-cytokeratin revealed fewer tumor foci within the DLN of mice treated with anti-CXCL13 or anti-CCL21 compared with control antibody-treated mice (Fig. 3C). Measurements of the total surface area of tumor foci (μm^2)

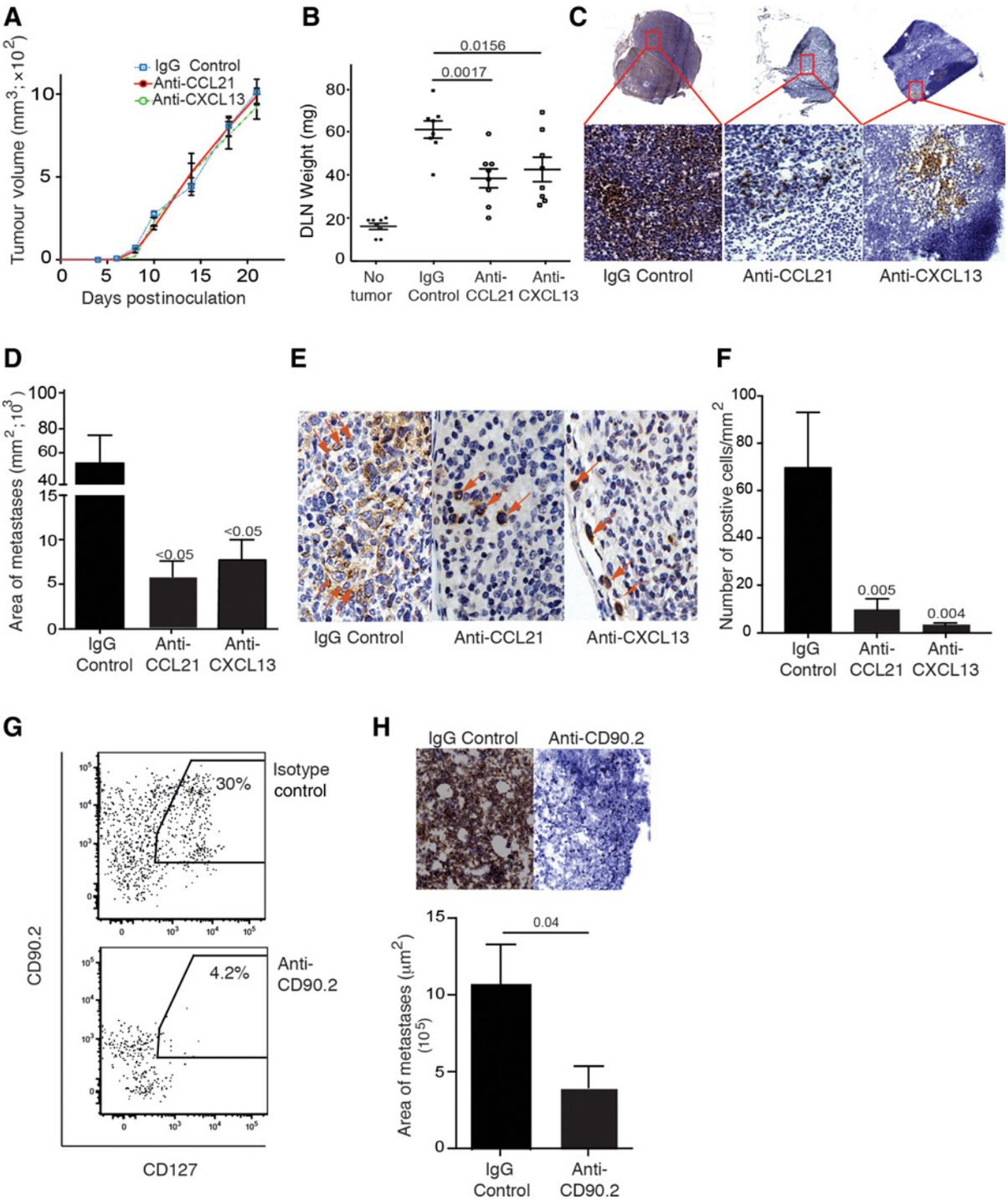

Figure 3.

CCL21, CXCL13, and ILCs promote metastasis of tumor cells to DLN. Tumor-bearing mice were treated with anti-CCL21, anti-CXCL13, or isotype control antibodies. $n = 6$ mice per treatment group. **A,** Tumor growth over time. **B,** Weight of inguinal DLN from mice at day 21. **C,** IHC of DLN from tumor-bearing BALB/c mice at day 21 using anti-pan-cytokeratin (brown). **D,** Quantification of the total area of metastasis per mm^2 of sectional area within lymph node at day 21. **E,** IHC of DLN from tumor-bearing $Rag1^{-/-}$ mice at day 21 using anti-pan-cytokeratin (brown). Orange arrows, pan-cytokeratin$^+$ tumor cells. **F,** Quantification of the total number of pan-cytokeratin$^+$ tumor cells/mm^2 of sectional area within lymph node at day 21 ($n \geq 3$ per group). **G,** FACS analysis for ILC in the DLN of isotype control and anti-CD90.2–treated $Rag1^{-/-}$ mice at day 14. Gating as in Fig. 1A. **H,** Pan-cytokeratin IHC (brown) of DLN of tumor-bearing $Rag1^{-/-}$ mice to assess tumor load in ILC-depleted (anti-CD90.2–treated) and nondepleted (isotype control–treated) mice at day 21 [bilateral tumors in three mice per treatment group ($n = 6$ per treatment group)]. The bar graphs show the total area of metastasis per mm^2 of sectional area within lymph node. Scale bar, 100 μm. Data, means ± SEM.

demonstrated a significant decrease in the tumor load in the DLN of mice treated with anti-CXCL13 or anti-CCL21 ($P < 0.05$ one-way ANOVA; Fig. 3C and D).

Given the involvement of CXCL13 and CCL21 in B- and T-cell homeostasis (2), we assessed the effect of anti-CXCL13 and anti-CCL21 blockade on lymph node metastasis in Rag1$^{-/-}$ mice, which lack B and T cells. Rag1$^{-/-}$ mice have much smaller lymph nodes; these lymph node samples were therefore formalin fixed to help preserve the morphology better. We report a decrease in the number of pan-cytokeratin positive tumor cells in DLN of tumor-bearing Rag1$^{-/-}$ mice treated with blocking anti-CCL21 or anti-CXCL13 (anti-CXCL13 $P = 0.004$; anti-CCL21 $P = 0.005$; Fig. 3E and F). These results suggest that T and B cells are not involved in the CXCL13- and CCL21-dependent tumor cell migration into lymph nodes.

To strengthen the link between ILC and chemokines in lymph node metastasis, we depleted ILCs with anti-CD90.2, as described previously (Fig. 3G; ref. 25). It is noteworthy that anti-CD90.2 does not specifically deplete ILC3 and is also able to deplete T cells. Therefore, these experiments were also carried out in Rag1$^{-/-}$ mice. We found a significant decrease in the tumor burden in the DLN of mice treated with anti-CD90.2 ($P = 0.04$ Mann–Whitney test; Fig. 3H). Therefore, CCL21, CXCL13, and ILCs themselves, and no B or T cells, all promote metastasis of breast cancer cells to the DLN.

CXCL13 induces RANK/RANKL signaling to promote tumor cell invasion

As our *in vivo* results suggested an inhibitory effect of CXCL13 or CCL21 blockade on 4T1.2 cell invasion into the DLN, we used ECM invasion assay to directly investigate the effects of increasing concentrations of CXCL13 and CCL21 on tumor cell invasion. EGF stimulation of 4T1.2 and NIH3T3 served as positive and negative controls, respectively. Recombinant CXCL13 or CCL21 did not significantly increase the invasion of 4T1.2 cells at concentrations between 10 and 100 ng/mL (Fig. 4A).

During lymph node development, the interaction of NKp46$^-$ILC3-MSC stimulates RANKL production by MSC, and RANKL signals back to the NKp46$^-$ILC3, establishing a positive feedback (26). CXCL13 has recently been shown to promote RANKL expression in stromal cells in oral squamous cell carcinoma (27), and RANK signaling in several breast cancer cell lines induces epithelial–mesenchymal transition (EMT), promoting cell migration and invasion (28). To test the relationship between CXCL13 and RANK signaling *in vitro*, we first confirmed, as shown previously (27), that although 4T.12 cells expressed RANK receptor *in vitro* (Fig. 4B), they were not themselves the source of RANKL (Fig. 4C). Levels of more than 200 pg/mL of RANKL were observed in MSC-conditioned media, supporting the hypothesis that the source of RANKL within the tumor is likely to be stromal (Fig. 4C). Stimulation with CXCL13, but not CCL21, increased the expression of RANKL in MSCs (paired *t* test 50 ng/mL vs. control: $P < 0.01$; Fig. 4D and E). We also confirmed that MSCs expressed CXCR5 as suggested by the above experiment (Supplementary Fig. S4). We next investigated whether increasing concentrations of RANKL would increase 4T1.2 cell invasion. Addition of RANKL to 4T1.2 (between 10 and 100 ng/mL) was observed to significantly increase the ability of the tumor cells to invade through the matrix (Fig. 4F).

To investigate the relationship between CXCL13 and RANKL expression *in vivo*, we analyzed the changes in the levels of RANKL in the sera of 4T1.2 tumor-bearing mice at a number of time points after tumor establishment. RANKL levels peaked at day 18 ($P < 0.0001$, unpaired *t* test; Fig. 4G), approximately 4 days after the first serum peak in CXCL13 (Fig. 1H). In mice treated with anti-CXCL13, levels of RANKL at day 14 were significantly reduced ($P < 0.001$ unpaired *t* test; Fig. 4H), in support of the idea that CXCL13 drives RANKL production *in vivo*. A significant reduction in RANKL was also observed in anti-CCL21–treated mice ($P < 0.001$ unpaired *t* test; Fig. 4H).

These findings led us to hypothesize that RANKL, like CCL21 and CXCL13, might promote metastasis of tumor cells to DLN. Treatment with anti-RANKL neutralizing antibody did not affect the growth of the primary tumor (Fig. 4I). Immunohistochemical analysis of DLN for tumor load revealed no metastasis in the majority of antibody-treated mice ($n = 5/7$), and the mean area of tumor metastasis was lower in the antibody-treated mice than the controls ($P < 0.01$, unpaired *t* test; Fig. 4J). RANKL blockade using a neutralizing antibody did not significantly affect the recruitment of NKp46$^-$ILC3 into the primary tumors, but the numbers in DLN were significantly lower, compared with the controls ($P < 0.05$, one-way ANOVA; Fig. 4K).

RORγt$^+$ILC and their associated chemokines are present in the human breast cancer TME

We further analyzed the gene expression of RORγt$^+$ILC3-associated/lymphoid chemokines CXCL13, CCL19, and CCL21 and their receptors, CXCR5 and CCR7, in a subset of 234 samples of breast cancer from the METABRIC (see Supplementary Table S3 for patient characteristics; ref. 29). Unsupervised hierarchical cluster analysis of the transcriptional profile in these samples revealed that this cohort could be categorized on the basis of their expression of RORγt$^+$ILC3-associated/lymphoid chemokines and their receptors (Fig. 5A). "Basal-like" breast cancers (PAM50-intrinsic subtype assignments; ref. 30) presented high expression of these genes (31/53 basal-like tumors lie in the top-branch cluster, $n = 89$; $P = 0.0007$, two-tailed Fisher exact test; Fig. 5A). Further cross-validation of these results was seen in four independent breast cancer datasets (Supplementary Fig. S5). RORγt$^+$ILC3-associated/lymphoid chemokine and their receptor genes were highly specific (no association with other lymphoid chemokine genes, such as the ligand–receptor pair CCL20–CCR6, which attracts immature DC, effector/memory T cells and B cells) and showed significant internal pairwise correlation ($P < 10^4$, Fig. 5B).

We next stained frozen primary tumor sections for markers for RORγt$^+$ILC3 (defined as RORγt$^+$CD127$^+$CD3$^-$), as we previously published (20). RORγt$^+$ILC3 were present in approximately half of the sections examined (Fig. 5C and D). These cells were in proximity to CD3$^+$ T cells (Fig. 5C) and found within tertiary lymphoid structures (TLS), as previously defined (Supplementary Fig. S6; ref. 31). We hypothesized that tumors with higher levels of RORγt$^+$ILC3-associated chemokines would have a higher number of RORγt$^+$ILC3. To test this, we performed a blinded study in primary breast cancer sections (total patients $n = 59$). The number of RORγt$^+$CD127$^+$CD3$^-$ cells/mm^2 (of total area/section) varied considerably from case to case (range, 0–56/mm^2; Fig. 5D), but patients with high tumor ILC3 counts were also likely to have a high gene expression score for the ILC3-associated chemokines (Fig. 5D; $P < 0.001$, Spearman correlation permutation test).

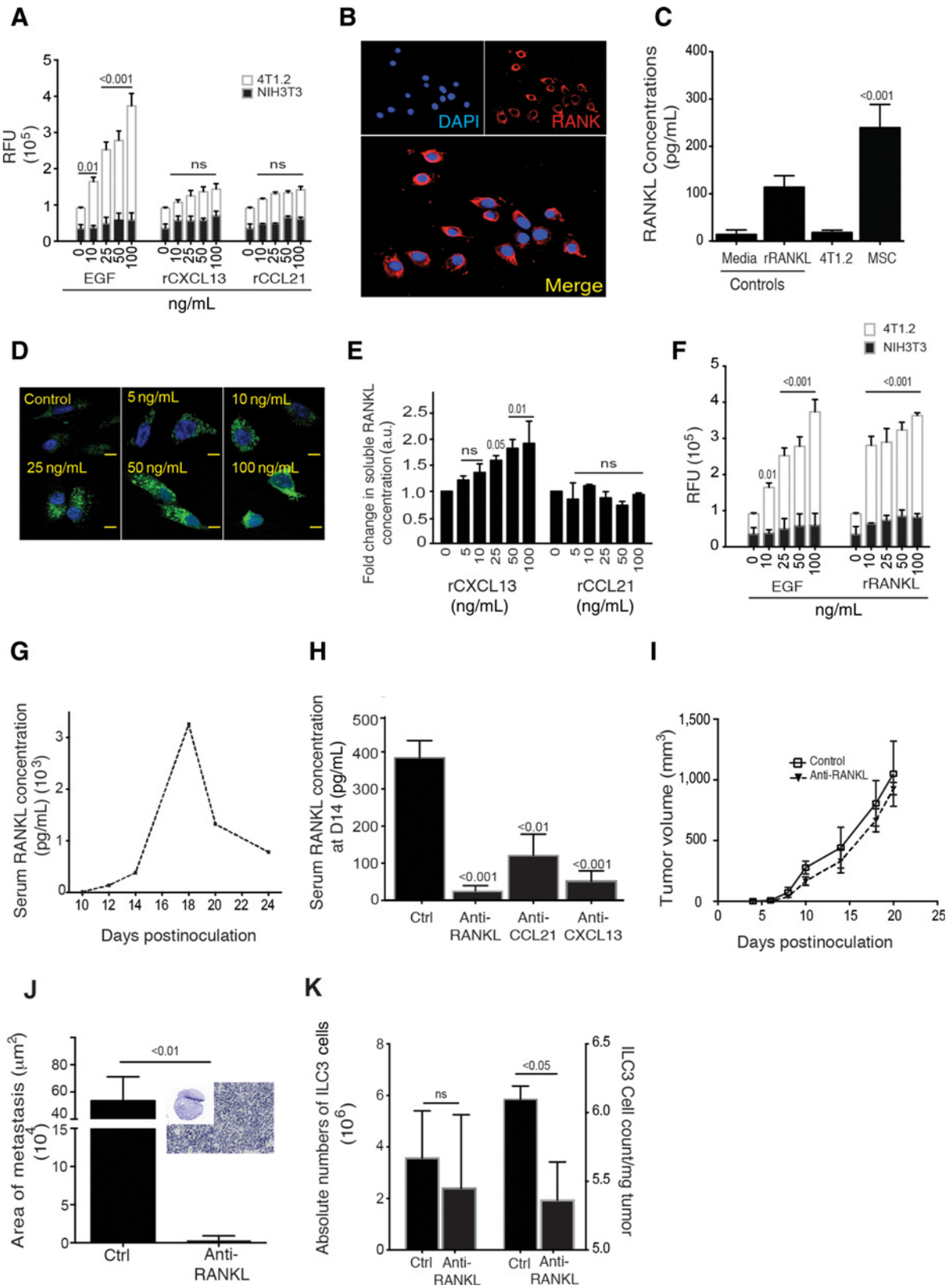

We next assessed the correlation of CXCL13 and CCL21 protein and gene expression levels with ILC3 scores. Fifty-nine cases with known ILC3 scores were stained for CXCL13 or CCL21 expression. For CXCL13, only stromal cells stained for this chemokine (Fig. 5E, i). In contrast, CCL21 staining was positive for both tumoral and stromal cells. We quantified the relationship between ILC3 and stromal CXCL13/CCL21 staining. ILC3 presence correlated positively with CXCL13 staining but not with stromal CCL21 (Fig. 5E, ii). These additional data strengthen our preclinical data (Fig. 2), with CXCL13 upregulation in stromal cells as a secondary event to the recruitment of ILC3 to the primary tumor.

Tumoral RORγt$^+$ILC3 cell density correlates with lymphatic tumor cell invasion and DLN metastasis within basal-like and HER2-enriched breast cancer

We next stained tumor sections for the lymphatic endothelial cell marker, podoplanin, and evaluated sections for evidence of tumor cell invasion into lymphatics (Fig. 6A, i). We considered lymphatic invasion to have occurred if at least one tumor cell cluster was clearly visible in the lymphatic vascular space (red arrow in Fig. 6A, i). RORγt$^+$ILC3 were present in 82% (14/17) of tumor samples with lymphatic tumor cell invasion but only in 27% (8/30) of samples without lymphatic tumor cell invasion. Similarly, 73% (22/30) of samples without lymphatic tumor cell invasion had no RORγt$^+$ILC3 present in the tumor, whereas only 17% (3/17) of samples without RORγt$^+$ILC3 cells displayed lymphatic invasion (Fig. 6, ii; $P < 0.003$, Fisher exact test). We did not find an association between lymphatic invasion and CD3$^+$ T cells or with CD3$^+$CD127$^+$RORγt$^+$ (most likely representing TH17 cells), strengthening the specificity of the correlation between RORγt$^+$ILC3 cells and lymphatic invasion (Supplementary Table S2). We next investigated whether the association between RORγt$^+$ILC3 counts and lymphatic invasion translated into a high lymph node tumor burden (i.e., four or more metastatic lymph nodes at surgical resection) within our dataset. In basal-like breast cancer, raised RORγt$^+$ILC3 counts were found to also correlate with a higher burden of lymph node metastases ($P = 0.02$, permutation-based Mann–Whitney; Fig. 6B). Given our *in vitro* and *in vivo* findings, we investigated whether lymph node burden was related to gene expression of CCL21 and CXCL13 in the primary tumor. We found that in basal-like breast cancers, a high lymph node tumor burden was associated with significantly increased levels of CCL21 ($P = 0.0043$; lymph node positive, 4+ vs. 0; two-tailed Mann–Whitney; Fig. 6C). Although CXCL13 levels were also increased in patients suffering from a high lymph node burden, this association was not significant ($P = 0.15$; Fig. 6D). These correlations were not statistically significant in other breast cancer subtypes (HER2$^+$ or luminal A/B), suggesting that the proposed mechanisms may only operate in specific breast cancer subtypes. In a multivariate (Cox) proportional hazards model and taking basal-like and HER2-enriched tumors together, the RORγt$^+$ILC3 score achieved 84% prediction accuracy for high lymph node burden, higher than traditional clinicopathologic parameters (e.g., grade, tumor size, receptor status; Fig. 6E).

Discussion

Recent years have seen a growing appreciation for the pleiotropic nature of the TME (32). The importance of ILC3s in normal lymphoid organogenesis has been accepted for a long time, but their role in the TME has only recently begun to be investigated. Work by Shields and colleagues described, in a murine model of melanoma, a mechanism by which CCL21-expressing tumors recruit ILC3 cells, which transform the TME contributing to a tolerant milieu that promotes immune evasion (21). Study by Eisenring and colleagues showed that RORγt$^+$ILCs are required for IL12 to exert its antitumor activity (33). Similarly, a protective function of NKp46$^+$ILC3 (distinct from the NKp46$^-$ILC3) has been reported in lung cancers (34). These findings are not necessarily at odds, as whether ILC3s promote or prevent cancer progression is likely to depend on the type of cancer and whether they recruit immune cells into a tolerogenic (21) or inflammatory (33) microenvironment. We report the presence of RORγt$^+$ILC3 in human breast cancers and that they have a previously unrecognized function in facilitating tumor invasion into the lymphatic system through modulation of the local lymphoid chemokine milieu. We show that ILC3 recruitment into a TNBC tumor model is CCL21 dependent, while CXCL13 regulates their clustering with stromal cells (see Fig. 7).

The CCL21/CCR7 axis plays a role in the progression of different malignancies (35, 36). These studies focus on the direct effects of CCL21 on CCR7-expressing tumor cells, rather than on how CCL21 may modify the TME. We show that CCL21 is expressed both in primary human breast cancers and in a mouse model of TNBC. In the mouse model, the peak of CCL21 expression in tumors was closely followed by ILC3 recruitment, an association we show to be causal through its prevention by CCL21 blockade, consistent with the melanoma xenograft study correlating tumor expression of CCL21 and ILC3 cell recruitment (21).

Figure 4.

CXCL13 induces RANK–RANKL signaling. **A,** Cell invasion assay with 4T1.2 cells (white bars) and NIH3T3 cells (black bars, noninvasive control). RFU, relative fluorescence unit. **B,** Confocal micrograph showing cytoplasmic and membranous staining of RANK (red) in 4T1.2 cells. Blue, DAPI-stained nuclei. **C,** Supernatants from coculture experiments of 4T1.2 cells and MSCs were analyzed after 48 hours to determine RANKL level by ELISA. **D**, RANKL expression in MSCs following stimulation by rCXCL13. Scale bar, 50 μm. **E,** RANKL concentration in MSC culture supernatants after stimulation with the indicated concentrations of rCXCL13 or rCCL21. a.u., arbitrary units. Data, means ± SEM, paired *t* test. **F,** Cell invasion assay, as described in **A**, with 4T1.2 stimulated with EGF and RANKL. Note: Data on **A** and **F** are the data from the same experiment. **G,** RANKL serum concentrations were determined at the indicated time points after tumor inoculation. ($n = 3$ mice/time point). **H**, RANKL serum concentration at day 14 in mice treated with neutralizing antibodies as indicated. Data, means ± SEM, unpaired *t* test. **I,** Tumor-bearing mice treated with either anti-RANKL or isotype control antibodies. The change in tumor volume with time after inoculation of 4T1.2 cells into the mammary fat pad is shown. **J,** Quantification of the total area of metastasis/mm^2 of sectional area in DLN of tumor-bearing mice treated with anti-RANKL or isotype control. Inset, representative IHC using anti-pan-cytokeratin (brown) to assess tumor burden in the anti-RANKL–treated cohort. **K,** Absolute cell counts of NKp46$^-$ILC3/mg of tumor and within DLN from tumor-bearing mice treated with anti-RANKL or isotype control antibody until day 21. ns, not significant. $n \geq 3$ mice/treatment group (one-way ANOVA. Data, means ± SEM, unpaired *t* test).

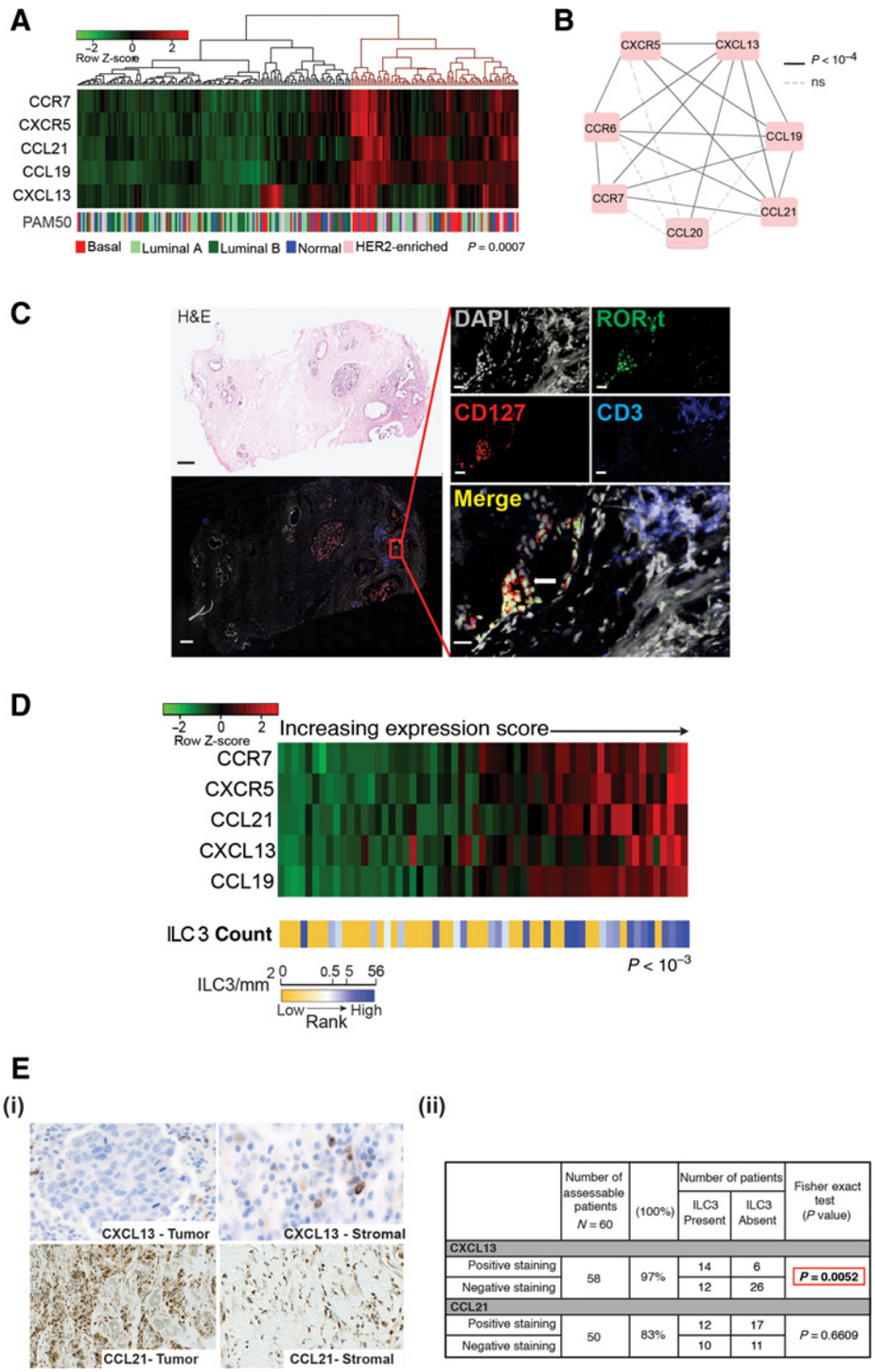

	Number of assessable patients N = 60	(100%)	Number of patients		Fisher exact test (P value)
			ILC3 Present	ILC3 Absent	
CXCL13					
Positive staining	58	97%	14	6	P = 0.0052
Negative staining			12	26	
CCL21					
Positive staining	50	83%	12	17	P = 0.6609
Negative staining			10	11	

Figure 5.

RORγt$^+$ILC3 and their associated chemokines in the human breast cancer TME. **A,** Hierarchical clustering of the expression of genes encoding lymphoid-associated chemokines and receptors in the Guy's METABRIC dataset ($N = 234$). Columns represent patient samples, with dendrogram colored according to the top-level cut-off point (black/red). PAM50-intrinsic subtype assignments are displayed below, and association was determined using a two-tailed Fisher exact test. **B,** Significance of pairwise gene expression correlations for genes encoding lymphoid-associated chemokines and receptors. **C,** Hematoxylin and eosin (H&E) staining and confocal micrographs of fresh-frozen section of a primary human breast cancer. RORγt$^+$ILC3 are defined as CD3$^-$CD127$^+$RORγt$^+$. Scale bar, 15 μm. **D,** Comparison of gene expression profiles and presence of RORγt$^+$ILC3. The heatmap illustrates relative expression of genes encoding RORγt$^+$ILC3-associated chemokines and receptors. Columns (samples, $n = 59$) are ordered by increasing expression score and rows by hierarchical clustering. The ranks of ILC3 counts (cells/mm^2) are depicted below, ordered from lowest to highest. **E, (i),** Immunohistochemical analysis for CXCL13 and CCL21 in human breast tumor samples; (**ii**) associations between stromal staining for CXCL13 or CCL21 and the presence/absence of RORγt$^+$ILC3. The association of these two cytokines and ILC3 was determined using Fisher exact test.

CXCL13 was not required for ILC3 recruitment to tumors but was important for the induction of ILC3–MSC clustering and RANKL upregulation by MSC. MSCs are recruited to tumors early in development via mechanisms reminiscent of those that operate in chronic wound healing (37, 38). Once activated, they secrete CXCL13, CCL21, and CCL19 and secrete lymphangiogenic factors, such as VEGF-C (39). This interaction, in the TME, may promote neo-lymphangiogenesis, increasing the number of lymphatic vessels into which tumor cells are able to migrate and thus increasing opportunities for lymphatic metastases.

In addition to its role in promoting clustering, CXCL13 stimulates increased RANKL production by MSC. This is likely to

A

(i)

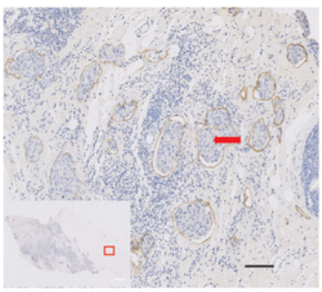

Lymphatic vessel invasion

(ii)

	Number of assessable patients $N = 60$	(100%)	Number of patients: Lymphatic invasion Absent	Present	Fisher exact test (P value)
CD3$^+$ Cells					
Low (<100/mm^2)	49	82%	18	8	$P = 0.1548$
High (>100/mm^2)			11	12	
CD3$^+$CD127$^+$RORγT$^+$ cells					
Absent	48	80%	26	12	$P = 0.1446$
Present			4	6	
ILC3 Cells					
Absent	47	78%	22	3	$P = 0.0003$
Present			8	14	

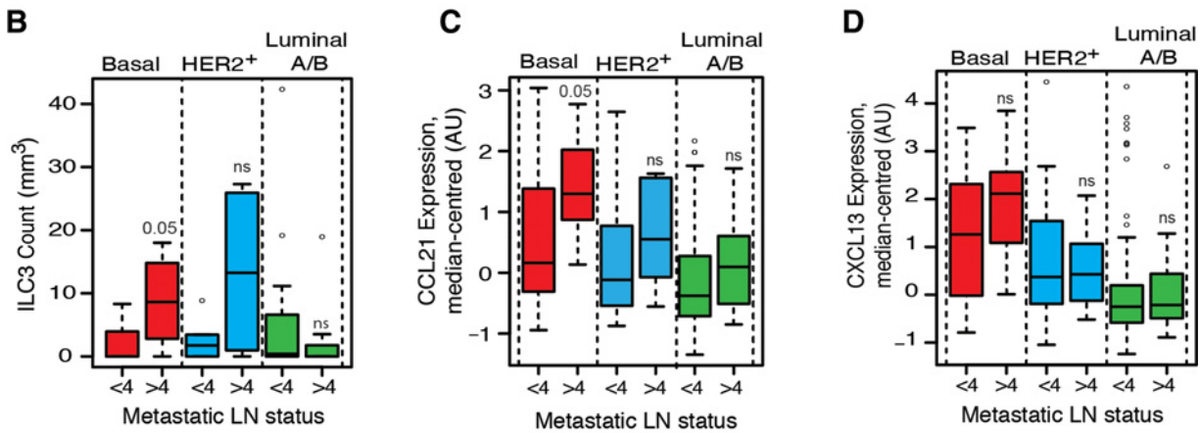

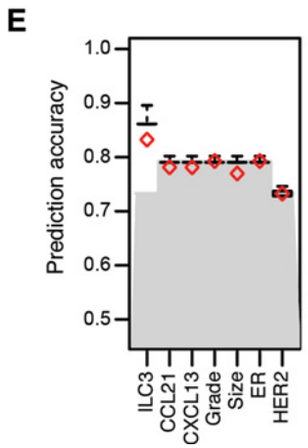

Figure 6.

Association of RORγt$^+$ILC3 and lymphatic invasion within the TME. **A, (i),** Immunohistochemical staining with lymphatic marker, podoplanin (brown) in primary human breast cancer tissue; cell nuclei are stained blue. Sections were examined for presence or absence of tumor cell invasion into lymphatics (red arrow) Scale bar, 100 μm; (**ii**) lymphatic invasion is associated with the presence of RORγt$^+$ILC3. The association between numbers of RORγt$^+$ILC3, CD3$^+$T cells or CD3$^+$CD127$^+$RORγt$^+$ cells with lymphatic invasion was determined using Fisher exact test. CD3-low was defined as <100 cells/mm^2, CD3-high as >100 cells/mm^2. **B**, Correlation between ILC3 count and the presence of lymphatic metastasis (Mann–Whitney *U* test is shown above the boxplots). ns, not significant. **C** and **D,** Correlation between CCL21 (**C**) and CXCL13 (**D**) gene expression and lymphatic metastasis in the METABRIC dataset. Median-centered gene expression values are shown (AU, arbitrary units). **E,** Prediction accuracy for lymph node (LN) burden among basal/HER2-enriched tumors. Average validation accuracy is shown (red diamonds). Baseline accuracy using assignment of all values to the largest class is shown for comparison (gray). RORγt$^+$ILC3/mm^2 achieves prediction accuracy of 84% using median threshold of 11.6/mm^2.

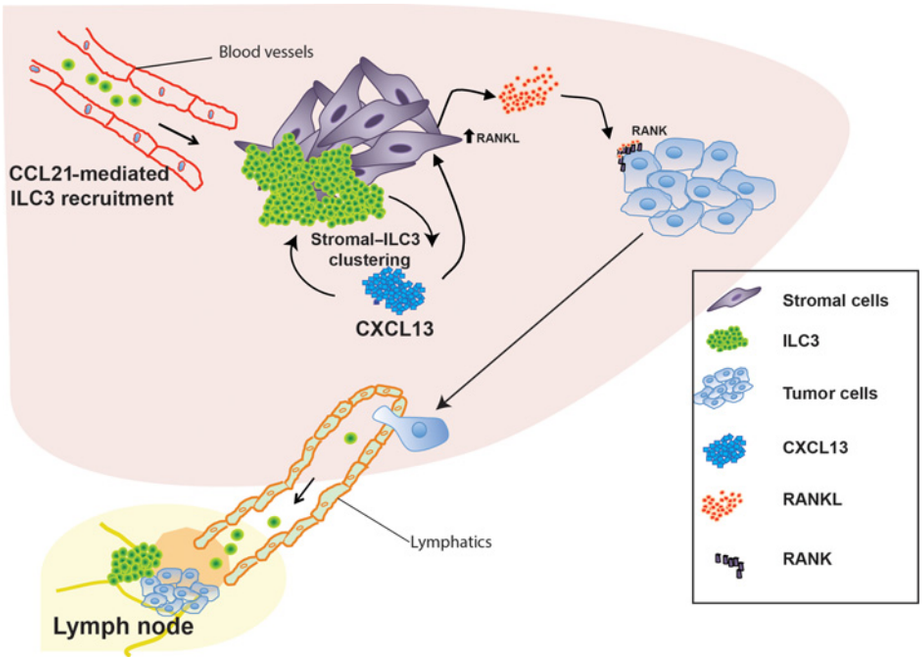

Figure 7.
In a model of TNBC, we report on the CCL21-mediated recruitment of ILC3 to tumors, where they stimulate stromal cells to produce CXCL13. CXCL13 feeds back to promote further interactions between ILC3 and stromal cells, leading to production of RANKL, which enhances tumor cell motility, resulting in lymph node metastases.

facilitate DLN metastasis by promoting EMT in breast cancer cells, enhancing their ability to migrate and metastasize (28, 40). This explains the reduction in serum levels of RANKL observed in anti-CXCL13–treated mice. ILC3 interaction with CXCL13-producing stromal cells may constitute a positive feedback, with CXCL13 reinforcing the ILC3–MSC interaction as shown *in vitro* and by intravital imaging. These are likely to explain our observations that patients with tumor cell invasion into the lymphatics were more likely to have a higher RORγt$^+$ILC3 score compared with patients without lymphatic vessel invasion, as well as the significant association between RORγt$^+$ILC3 counts and greater risk of an increased number of lymph node metastasis in basal-like breast cancer patients.

CXCL13 is highly expressed in clinical samples from some breast cancer patients (41), but there is conflicting evidence on how it affects disease progression. Although high CXCL13–CXCR5 expression positively correlates with classical determinants of poor prognosis (41, 42), it serves as a good prognostic marker within this high-risk subgroup of breast cancer patients (42–44). Within the TME, the role of immune cells and/or chemokines is particularly complex (45, 46). Here, we report that downstream of CCL21-mediated recruitment of intratumoral ILC3, CXCL13 promotes lymphatic invasion of tumor cells via the RANK–RANKL signaling pathway. However, CXCL13 is also a powerful chemoattractant for lymphocytes (47). This is in line with our finding that basal-like breast cancers, which frequently bear a prominent lymphocytic infiltrate, presented a high score for the lymphoid chemokine/chemokine receptor gene signature, and our data demonstrating a decreased number of tumor-infiltrating lymphocytes (TIL) in anti-CCL21- or anti-CXCL13–treated mice. In addition, TILs and TLS are described as key prognostic and predictive markers for specific breast cancer subtypes (47–50). Therefore, the well-established role of CXCL13 as a chemoattractant could explain why, in a subset of cases, it seems to play a protective role. In our cohort of patients, CCL21 expression and RORγt$^+$ILC3 presence in the primary tumor were associated with increased DLN metastasis in basal-like breast cancer, but not in HER2$^+$ or luminal A/B subtypes. It is noteworthy that these data may not translate into worse prognosis for patients, and additional studies are required to fully understand the clinical significance of these findings.

One important consideration for any future development of chemokine-based therapeutic interventions is the interplay between the CCL19–CCL21/CCR7 and CXCL13/CXCR5 axes within tumors. Both have been implicated as important drivers of leukocyte trafficking and lymphoid organogenesis in physiologic situations (51). However, it is important to make a distinction between the two chemokines in the pathologic context of the TME as CXCL13, but not CCL21, is required for ILC3–MSC clustering, which we proposed here to be an important regulatory mechanism in tumor cell migration through RANKL production by MSC.

In summary, we propose that, in our tumor model, ILC3s are recruited to the tumor by CCL21, have a pivotal role in facilitating lymphatic vessel invasion by tumor cells, and they do this via two CXCL13-mediated positive feedback loops. Further investigation into how ILC3, MSC, CCL21, CXCL13, and RANKL are coordinated to establish a network of interactions between the tumor cells and their microenvironment is required.

Disclosure of Potential Conflicts of Interest

No potential conflicts of interest were disclosed.

Authors' Contributions

Conception and design: S. Irshad, F. Flores-Borja, S.A. Quezada, A.N.J. Tutt, T. Ng

Development of methodology: S. Irshad, F. Flores-Borja, V. Male, G.O. Fruhwirth, S. Ameer-Beg, L.M. Carlin, D.R. Withers, B. Vojnovic

Acquisition of data (provided animals, acquired and managed patients, provided facilities, etc.): S. Irshad, F. Flores-Borja, J. Monypenny, R. Evans, V. Male, P. Gordon, A. Cheung, P. Gazinska, F. Noor, F. Wong, P.R. Barber, N. Woodman, D. Patel, J. Owen, S.G. Martin, S.E. Pinder, C.E. Gillett, S.P. Poland, F. McCaughan, L.M. Carlin, B. Vojnovic

Analysis and interpretation of data (e.g., statistical analysis, biostatistics, computational analysis): S. Irshad, F. Flores-Borja, K. Lawler, R. Evans, V. Male, A. Grigoriadis, G.O. Fruhwirth, M. Rodriguez-Justo, D.R. Withers, P. Lane, B. Vojnovic, S.A. Quezada, P. Ellis

Writing, review, and/or revision of the manuscript: S. Irshad, F. Flores-Borja, V. Male, G.O. Fruhwirth, S.G. Martin, S.E. Pinder, U. Hasan, S.A. Quezada, P. Ellis, A.N.J. Tutt, T. Ng

Administrative, technical, or material support (i.e., reporting or organizing data, constructing databases): S. Irshad, N. Woodman, D. Patel, M. Rodriguez-Justo, J. Owen, S. Ameer-Beg

Study supervision: S. Ameer-Beg, A.N.J. Tutt, T. Ng

The costs of publication of this article were defrayed in part by the payment of page charges. This article must therefore be hereby marked *advertisement* in accordance with 18 U.S.C. Section 1734 solely to indicate this fact.

Received April 20, 2016; revised December 9, 2016; accepted December 10, 2016; published OnlineFirst January 12, 2017.

References

1. Mohammed RA, Ellis IO, Mahmmod AM, Hawkes EC, Green AR, Rakha EA, et al. Lymphatic and blood vessels in basal and triple-negative breast cancers: characteristics and prognostic significance. Mod Pathol 2011;24:774–85.
2. Stein JV, Nombela-Arrieta C. Chemokine control of lymphocyte trafficking: a general overview. Immunology 2005;116:1–12.
3. Ansel KM, Ngo VN, Hyman PL, Luther SA, Forster R, Sedgwick JD, et al. A chemokine-driven positive feedback loop organizes lymphoid follicles. Nature 2000;20;406:309–14.
4. Ohl L, Henning G, Krautwald S, Lipp M, Hardtke S, Bernhardt G, et al. Cooperating mechanisms of CXCR5 and CCR7 in development and organization of secondary lymphoid organs. J Exp Med 2003;197:1199–204.
5. van de Pavert SA, Olivier BJ, Goverse G, Vondenhoff MF, Greuter M, Beke P, et al. Chemokine CXCL13 is essential for lymph node initiation and is induced by retinoic acid and neuronal stimulation. Nat Immunol 2009;10:1193–9.
6. Spits H, Artis D, Colonna M, Diefenbach A, Di Santo JP, Eberl G, et al. Innate lymphoid cells–a proposal for uniform nomenclature. Nat Rev Immunol 2013;13:145–9.
7. Sun Z, Unutmaz D, Zou YR, Sunshine MJ, Pierani A, Brenner-Morton S, et al. Requirement for RORgamma in thymocyte survival and lymphoid organ development. Science 2000;288:2369–73.
8. Tsuji M, Suzuki K, Kitamura H, Maruya M, Kinoshita K, Ivanov II, et al. Requirement for lymphoid tissue-inducer cells in isolated follicle formation and T cell-independent immunoglobulin A generation in the gut. Immunity 2008;29:261–71.
9. Scandella E, Bolinger B, Lattmann E, Miller S, Favre S, Littman DR, et al. Restoration of lymphoid organ integrity through the interaction of lymphoid tissue-inducer cells with stroma of the T cell zone. Nat Immunol 2008;9:667–75.
10. Honda K, Nakano H, Yoshida H, Nishikawa S, Rennert P, Ikuta K, et al. Molecular basis for hematopoietic/mesenchymal interaction during initiation of Peyer's patch organogenesis. J Exp Med 2001;193:621–30.
11. Weigelt B, Mackay A, A'Hern R, Natrajan R, Tan DS, Dowsett M, et al. Breast cancer molecular profiling with single sample predictors: a retrospective analysis. Lancet Oncol 2010;11:339–49.
12. Parker JS, Mullins M, Cheang MC, Leung S, Voduc D, Vickery T, et al. Supervised risk predictor of breast cancer based on intrinsic subtypes. J Clin Oncol 2009;27:1160–7.
13. Gazinska P, Grigoriadis A, Brown JP, Millis RR, Mera A, Gillett CE, et al. Comparison of basal-like triple-negative breast cancer defined by morphology, immunohistochemistry and transcriptional profiles. Mod Pathol 2013;26:955–66.
14. Withers DR, Gaspal FM, Mackley EC, Marriott CL, Ross EA, Desanti GE, et al. Cutting edge: lymphoid tissue inducer cells maintain memory CD4 T cells within secondary lymphoid tissue. J Immunol 2012;189:2094–8.
15. Lelekakis M, Moseley JM, Martin TJ, Hards D, Williams E, Ho P, et al. A novel orthotopic model of breast cancer metastasis to bone. Clin Exp Metastasis 1999;17:163–70.
16. Kedrin D, Gligorijevic B, Wyckoff J, Verkhusha VV, Condeelis J, Segall JE, et al. Intravital imaging of metastatic behavior through a mammary imaging window. Nat Methods 2008;5:1019–21.
17. Hothorn T, Hornik H, van de Wiel MA, Zeileis A. A lego system for conditional inference. Am Stat 2006;60:257–63.
18. Kaur P, Nagaraja GM, Zheng H, Gizachew D, Galukande M, Krishnan S, et al. A mouse model for triple-negative breast cancer tumor-initiating cells (TNBC-TICs) exhibits similar aggressive phenotype to the human disease. BMC Cancer 2012;12:120.
19. Walker JA, Barlow JL, McKenzie AN. Innate lymphoid cells–how did we miss them? Nat Rev Immunol 2013;13:75–87.
20. Kim S, Han S, Withers DR, Gaspal F, Bae J, Baik S, et al. CD117(+) CD3(-) CD56(-) OX40Lhigh cells express IL-22 and display an LTi phenotype in human secondary lymphoid tissues. Eur J Immunol 2011;41:1563–72.
21. Shields JD, Kourtis IC, Tomei AA, Roberts JM, Swartz MA. Induction of lymphoidlike stroma and immune escape by tumors that express the chemokine CCL21. Science 2010;328:749–52.
22. Brendolan A, Caamano JH. Mesenchymal cell differentiation during lymph node organogenesis. Front Immunol 2012;3:381.
23. Evans I, Kim MY. Involvement of lymphoid inducer cells in the development of secondary and tertiary lymphoid structure. BMB Rep 2009;42:189–93.
24. Bernardo ME, Locatelli F, Fibbe WE. Mesenchymal stromal cells. Ann N Y Acad Sci 2009;1176:101–17.
25. Monticelli LA, Sonnenberg GF, Abt MC, Alenghat T, Ziegler CG, Doering TA, et al. Innate lymphoid cells promote lung-tissue homeostasis after infection with influenza virus. Nat Immunol 2011;12:1045–54.
26. Mueller CG, Hess E. Emerging functions of RANKL in lymphoid tissues. Front Immunol 2012;3:261.
27. Sambandam Y, Sundaram K, Liu A, Kirkwood KL, Ries WL, Reddy SV. CXCL13 activation of c-Myc induces RANK ligand expression in stromal/preosteoblast cells in the oral squamous cell carcinoma tumor-bone microenvironment. Oncogene 2013;32:97–105.
28. Palafox M, Ferrer I, Pellegrini P, Vila S, Hernandez-Ortega S, Urruticoechea A, et al. RANK induces epithelial-mesenchymal transition and stemness in human mammary epithelial cells and promotes tumorigenesis and metastasis. Cancer Res 2012;72:2879–88.
29. Curtis C, Shah SP, Chin SF, Turashvili G, Rueda OM, Dunning MJ, et al. The genomic and transcriptomic architecture of 2,000 breast tumours reveals novel subgroups. Nature 2012;486:346–52.
30. Perou CM, Sorlie T, Eisen MB, van de Rijn M, Jeffrey SS, Rees CA, et al. Molecular portraits of human breast tumours. Nature 2000;406:747–52.
31. Pages F, Galon J, Dieu-Nosjean MC, Tartour E, Sautes-Fridman C, Fridman WH. Immune infiltration in human tumors: a prognostic factor that should not be ignored. Oncogene 2010;29:1093–102.
32. Quail DF, Joyce JA. Microenvironmental regulation of tumor progression and metastasis. Nat Med 2013;19:1423–37.
33. Eisenring M, vom Berg J, Kristiansen G, Saller E, Becher B. IL-12 initiates tumor rejection via lymphoid tissue-inducer cells bearing the natural cytotoxicity receptor NKp46. Nat Immunol 2010;11:1030–8.
34. Carrega P, Loiacono F, Di Carlo E, Scaramuccia A, Mora M, Conte R, et al. NCR(+)ILC3 concentrate in human lung cancer and associate with intratumoral lymphoid structures. Nat Commun 2015;6:8280.
35. Mashino K, Sadanaga N, Yamaguchi H, Tanaka F, Ohta M, Shibuta K, et al. Expression of chemokine receptor CCR7 is associated with lymph node metastasis of gastric carcinoma. Cancer Res 2002;62:2937–41.
36. Muller A, Homey B, Soto H, Ge N, Catron D, Buchanan ME, et al. Involvement of chemokine receptors in breast cancer metastasis. Nature 2001;410:50–6.

37. Spaeth E, Klopp A, Dembinski J, Andreeff M, Marini F. Inflammation and tumor microenvironments: defining the migratory itinerary of mesenchymal stem cells. Gene Ther 2008;15:730–8.
38. Dvorak HF. Tumors: wounds that do not heal. Similarities between tumor stroma generation and wound healing. N Engl J Med 1986;315:1650–9.
39. Benezech C, White A, Mader E, Serre K, Parnell S, Pfeffer K, et al. Ontogeny of stromal organizer cells during lymph node development. J Immunol 2010;184:4521–30.
40. Biswas S, Sengupta S, Roy Chowdhury S, Jana S, Mandal G, Mandal PK, et al. CXCL13-CXCR5 co-expression regulates epithelial to mesenchymal transition of breast cancer cells during lymph node metastasis. Breast Cancer Res Treat 2014;143:265–76.
41. Panse J, Friedrichs K, Marx A, Hildebrandt Y, Luetkens T, Barrels K, et al. Chemokine CXCL13 is overexpressed in the tumour tissue and in the peripheral blood of breast cancer patients. Br J Cancer 2008;99:930–8.
42. Razis E, Kalogeras KT, Kotoula V, Eleftheraki AG, Nikitas N, Kronenwett R, et al. Improved outcome of high-risk early HER2 positive breast cancer with high CXCL13-CXCR5 messenger RNA expression. Clin Breast Cancer 2012;12:183–93.
43. Yau C, Esserman L, Moore DH, Waldman F, Sninsky J, Benz CC. A multigene predictor of metastatic outcome in early stage hormone receptor-negative and triple-negative breast cancer. Breast Cancer Res 2010;12:R85.
44. Sabatier R, Finetti P, Mamessier E, Raynaud S, Cervera N, Lambaudie E, et al. Kinome expression profiling and prognosis of basal breast cancers. Mol Cancer 2011;10:86.
45. DeNardo DG, Andreu P, Coussens LM. Interactions between lymphocytes and myeloid cells regulate pro- versus anti-tumor immunity. Cancer Metastasis Rev 2010;29:309–16.
46. Viola A, Sarukhan A, Bronte V, Molon B. The pros and cons of chemokines in tumor immunology. Trends Immunol 2012;33:496–504.
47. Gu-Trantien C, Loi S, Garaud S, Equeter C, Libin M, de Wind A, et al. CD4+ follicular helper T cell infiltration predicts breast cancer survival. J Clin Invest 2013;123:2873–92.
48. Loi S, Sirtaine N, Piette F, Salgado R, Viale G, Van Eenoo F, et al. Prognostic and predictive value of tumor-infiltrating lymphocytes in a phase III randomized adjuvant breast cancer trial in node-positive breast cancer comparing the addition of docetaxel to doxorubicin with doxorubicin-based chemotherapy: BIG 02–98. J Clin Oncol 2013;31:860–7.
49. Denkert C, Loibl S, Noske A, Roller M, Muller BM, Komor M, et al. Tumor-associated lymphocytes as an independent predictor of response to neoadjuvant chemotherapy in breast cancer. J Clin Oncol 2010;28:105–13.
50. Ono M, Tsuda H, Shimizu C, Yamamoto S, Shibata T, Yamamoto H, et al. Tumor-infiltrating lymphocytes are correlated with response to neoadjuvant chemotherapy in triple-negative breast cancer. Breast Cancer Res Treat 2012;132:793–805.
51. Cyster JG. Chemokines and cell migration in secondary lymphoid organs. Science 1999;286:2098–102.